Comparison of HYCOM and POP Ocean Models in the CCSM3.0 Framework

Part I: Understanding Model Biases from Modes of Climate Variability

Jianhua Lu[1], Eric P. Chassignet[1, 2], Jianjun Yin[3], Vasubandhu Misra[1, 2], John-Paul Michael[1,2]

1Center for Ocean-Atmospheric Prediction Center,

2 Department of Earth, Ocean and Atmospheric Science,

Florida State University, Tallahassee, Florida

3 Department of Geosciences, University of Arizona, Tucson, Arizona

Corresponding Author and Email Address:

Jianhua Lu

jlu@coaps.fsu.edu

Abstract

Coupled climate simulations are performed with the Community Climate System Model version 3 (CCSM3) configuration, but with two different ocean models: the default depth-coordinate Parallel Ocean Program (POP) model in the CCSM3 and the primarily isopycnal HYbrid Coordinate Ocean Model (HYCOM). To gain some understanding of the model biases, the mean climate and modes of climate variability of the two models are compared with observations. The examination includes the Northern and Southern Annular Modes (NAM and SAM), the Pacific-North-American (PNA) pattern, the Atlantic Multidecadal Oscillation (AMO), and the main Southern Ocean SST mode. It is found that (1) the NAM modes in the two models show a systematic shift of atmospheric jets, precipitation, and eddy activities to the east of the observations, and the simulated centers of the NAM over the North Pacific are stronger than in the observations. This systematic eastward shift of the NAM can be related to the mean SST biases in the North Atlantic through interaction between the mean flow and the synoptic eddies; (2) over the Southern Ocean, the SSTs shows warm biases in the CCSM3/HYCOM and cold biases in CCSM3/POP. The model biases in the dominant mode of SST variability over the Southern Ocean partly originate from the biases in the tropics; (3) in contrast to the patterns in CCSM3/POP and the observations, the PNA pattern in CCSM3/HYCOM has no correlation with El Niño-Southern Oscillation (ENSO) in CCSM3/HYCOM, suggesting the PNA pattern can be a mode of internal variability in the extratropics, rather than being forced by ENSO. The comparisons presented in the paper highlight the importance of ocean model vertical coordinates and

representation of physical processes in climate simulation through their non-local influence on modes of climate variability.

1 Introduction

With more than two -decades of community-wide efforts, the Community Climate System Model (CCSM) has been developed into one of the most frequently used climate models for global climate change research (e.g. Gent et al. 2011). The CCSM framework comprises, among many other components, models of the physical climate system that include atmosphere, land surface, ocean, and sea ice, which are coupled as an integrated system. The CCSM3, released in 2004, featured a major improvement in the model's numerical and software architecture and physics and consequently, an improvement in its climate simulation performance, which was documented in a special issue of the *Journal of Climate* published in 2006 (Collins et al. 2006). The CCSM3 was a major player in the Coupled Model Intercomparison Project 3 (CMIP3). The version 4 of CCSM and its earth system model version (CESM1) have been released recently (Gent et al. 2011).

The development of the CCSM, particularly the atmospheric model of the CCSM (CAM), has benefited from the use of different dynamic cores and physical parameterizations (Jablonowski and Williamson 2006). While the officially released atmospheric component of CCSM3 and CCSM4 models is on a pressure-based $\sigma - p$ coordinate, the recent implementation of a hybrid isentropic-σ coordinate in the FV dynamical core of CAM has shown significant improvement in the simulated climate, such as the reduction of the long-standing cold pole problem, illustrating the importance of the choice of vertical discretization in a GCM (Chen and Rasch, 2011).

The ocean component of the CCSM lacks similar diversity in its configuration, especially in its choice of vertical coordinates and dynamic cores as in the CAM. The officially adopted ocean component of the CCSM, the Parallel Ocean Program (POP) and its latest version POP2, developed at Los Alamos National Laboratory, is a depth-based, level-coordinate ocean general circulation model (Smith et al. 1992; Danabasoglu et al. 2011). However, in the coupled climate modeling community the lack of diversity in the ocean models, especially when compared to their atmospheric counterparts, has recently been alleviated by the introduction of isopycnal or hybrid vertical coordinates (McAvaney et al. 2001). Coupled simulations performed with ocean models that use isopycnal or hybrid coordinates in the vertical have been shown to produce solutions that are comparable to those obtained with the more common depth coordinates (Randall et al. 2007; Griffies et al. 2009). The use of isopycnal/hybrid coordinates reduces the amount of spurious diapycnal mixing and facilitates the treatment of bottom topography (see Chassignet 2011 for a thorough review on the isopycnal and hybrid coordinates). Isopycnic coordinate models are ideally suited for representing interior ocean transport, especially for climate simulations on decadal and longer time scales.

The latest version of the Hybrid Coordinate Ocean Model (HYCOM2.2) was implemented in the CCSM3 framework to increase the structural diversity of the ocean component in the CCSM framework. In this paper, we compare the differences in mean climate and modes of climate variability in the simulations using two different ocean models under the same CCSM3 framework. The use of two ocean models is useful in identifying the source of model biases. For example, the different features in model biases may stem from the model structures, such as the vertical coordinate choices.

Biases can result from different sources in the coupled model simulations: model resolution and numerics, uncertainty in representation of physical processes and subgrid-scale parameterizations, etc. At the present time, it is unclear which component (ocean, atmosphere, or their coupling) of coupled climate models leads to these biases and to what extent the biases are caused by the coarse horizontal resolution or choice of vertical coordinate, parameterization of atmospheric processes, or the parameterization of oceanic processes. Gent et al. (2010) showed that the warm SST biases in the major upwelling regions are reduced by as much as 60% in a 0.5°° resolution of the atmospheric model of CCSM3.5 (an interim version) compared to a 2.0° horizontal resolution version of the atmospheric model. They attributed this improvement at 0.5° resolution to better interaction of the surface atmospheric flow with orography and improved resolution of the atmospheric baroclinic eddies. Furthermore, Gent et al. (2010) showed that higher resolution of the atmospheric model also leads to improvements in precipitation over the Asian monsoon and the eastern tropical Pacific regions, and in annual river discharge into the Atlantic Ocean.

However, model resolution is not the only source for bias, as also stated by Gent et al. (2010). The 0.5° resolution in the atmosphere/land model has no effect on important biases such as the double ITCZ in the tropical Pacific and the cold SST bias in the North Atlantic. Furthermore there is only marginal improvement in the sea surface salinity (SSS) simulation at 0.5° resolution. In fact the spatial pattern and the magnitude of the SSS bias are similar in the 0.5° and 2.0° resolution simulations (Fig. 6 in Gent et al. 2010). It is well known that model biases can also result from discrepancies and uncertainties in the parameterizations, and therefore the parameterization improvements may reduce the model biases. The new parameterizations of atmospheric and oceanic processes adopted in the latest versions of CCSM and CESM (e.g. Neale et al. 2008;

Danabasoglu et al. 2008) and the evaluations of the new parameterizations reflect the efforts of the modeling community in earth system model development.

A common method in reducing the biases in model development and validation is to compare the model mean climate with the observations. However, the comparison of the mean climate reveals only part of the model biases and is limited in its ability to unravel the mechanical and non-local linkage between the representation of model processes and the model biases. Take the SST bias in high latitudes as an example. It is intuitive to adjust the model parameters (such as mixing coefficient) locally to reduce the model bias, but physically the bias may well be caused by the misrepresentation of the tropical processes. On the other hand, the change of model parameter in high latitudes may also induce the non-local effects on the tropical climate. In this regard, the comparison of the modes of climate variability is particularly beneficial to model development because the dynamical and statistical diagnostics of these modes in both models and observations may help reveal the physical processes through which the model structure and parameterization affect the coupled simulation. The comparison may also reveal the non-local relations between the various climate variables (such as tropical SST, precipitation, wind, etc.) associated with these modes. Although the underlying mechanisms may be different, the biases in the mean model climate and the associated modes of climate variability may be closely inter-linked through the nonlinear interaction between mean flow and these (high or low frequency) modes.

With these considerations in mind, in Part I we first compare the mean bias in SST and SSS in the CCSM3/HYCOM and the standard CCSM3/POP simulations. This is followed with comparing some of the well-known modes of climate variability in the atmosphere and ocean in CCSM3/HYCOM and the standard CCSM3/POP to those derived from the NCEP/NCAR reanalysis and from the latest version of the Extended Reynolds Sea Surface Temperature (ERSST) data. The atmospheric modes analyzed are the Northern and Southern annular modes (NAM and SAM) and the Pacific-North-American (PNA) pattern. The oceanic modes in the Atlantic and in the Southern Ocean SST are also investigated. We have chosen these modes not only because they are dominant modes in the coupled physical climate system, but also because some of these modes (such as NAM and SAM) provide mechanical and fresh-water forcings to the ocean circulation and its variability, which potentially in turn forces some of the atmospheric modes of variability. Therefore, the diagnosis of these modes is suitable to directly reveal the difference in coupled ocean-atmospheric interactions caused by the use of two ocean models in the same CCSM3 framework. Part II, a companion paper, addresses the fidelity of ENSO simulation in the two models (Michael et al. 2012).

We find from the model comparisons in this study, that the NAM modes in the two models display a systematic shift of atmospheric jets, precipitation, and eddy activities to the east of the observations, and the simulated centers of the NAM over the North Pacific are stronger than in the observations. This systematic eastward shift of the NAM can be related to the mean SST biases in the North Atlantic that influences the through interaction between the mean flow and the synoptic eddies. We also find that over the Southern Ocean, the SST shows warm bias in the CCSM3/HYCOM and cold bias in CCSM3/POP. The model biases in the dominant mode of SST variability over the Southern Ocean partly originate from the biases in the tropics. In contrast to the PNA patterns in CCSM3/POP and the observations, the PNA pattern in CCSM3/HYCOM has no correlation with El Niño and the Southern Oscillation (ENSO), suggesting that the PNA pattern can be a mode of internal variability in the extratropics.

The organization of the paper is as follows. In Section 2 the model configurations of HYCOM2.2 and POP in the CCSM3 framework are briefly introduced and then the modeled mean SST and SSS are compared. Section 3 discusses the comparison of the dominant atmospheric modes, including the NAM, SAM, and the PNA pattern. In Section 4 we compare the SST modes in the Atlantic and the Southern Ocean in the model simulations and observations. Finally, a summary and discussion are provided in Section 5. The comparison of ENSO simulations with the observations is the topic of a companion paper by Michael et al. (2012).

2 Ocean Model Configuration and the Mean Climate

A full overview of and detailed information about the POP ocean model in CCSM3 is available in Collins et al. (2006) and Danabasoglu et al. (2006). Here we provide only a brief introduction. The POP model in the CCSM3 used in this study has a dipole grid with a nominal 1° horizontal resolution. The first pole is located at the South Pole and the second pole is located over Greenland. The vertical coordinate has 40 levels extending to 5.37 km. The horizontal grid (gx1v3 grid) has 320 zonal points and 384 meridional points, and the spacing of the grids is 1.125° in the zonal direction and roughly 0.5° in the meridional direction, with higher resolution in the tropics. The sea ice model is integrated on the same horizontal grid as the ocean model.

The default configuration of HYCOM is isopycnic in the open stratified ocean, but it makes a dynamically and geometrically smooth transition to terrain-following coordinates in shallow coastal regions and to fixed pressure-level coordinates in the surface mixed layer and/or unstratified open seas. In doing so, the model takes advantage of the different coordinate types in optimally simulating coastal and open-ocean circulation features. Numerically induced cross-isopycnal mixing is mostly eliminated in isopycnic coordinate modeling. There are 32 hybrid vertical layers, with the target isopycnal density ranging from 28.10 to 37.25 kg/m^3. The HYCOM used in the present study is the latest version 2.2 (hereafter, HYCOM2; http://www.hycom.org). It uses the same horizontal grid (gx1v3 grid) as the POP except that HYCOM uses a staggered Arakawa-C grid whereas POP uses a Arakawa-B grid (Bleck 2002; Chassignet et al. 2003). The baroclinic and barotropic time steps of HYCOM2 are 2160 s and 36 s, respectively. HYCOM2 is equipped with several vertical mixing schemes, with the standard version using a non-slab K-profile parameterization (KPP) mixed layer submodel (Large et al. 1994). As in POP, virtual salt flux is employed at the ocean surface. HYCOM2 has been integrated with the CCSM3 coupler version 6 so that different configurations of CCSM3/HYCOM can follow the standard procedure of CCSM3. All the component models except the ocean component remain the same as in the standard CCSM3. The coupled CCSM3/HYCOM has been integrated for 400 years with the standard present-day (1990) forcing used in the CCSM3 present-day control experiment for phase 3 of the Coupled Model Intercomparison Project (CMIP3). We use the output of the last 200 years for the diagnosis. Similarly, the last 200-year monthly mean data for the CCSM3/POP simulation, downloaded from CMIP3 database (http://www-pcmdi.llnl.gov/), are used for the comparison.

Figure 1 shows a comparison of the SST biases in the coupled CCSM3/HYCOM runs with the standard CCSM3/POP runs relative to the observed SST. Similar SST biases between CCSM3/HYCOM and CCSM3/POP include a warm SST bias along the western coasts of the continents (the major upwelling regions), which extends westward into the middle of the ocean basins, and a cold SST bias in the Northern Atlantic. Gent et al. (2010) showed that the warm SST biases in the major upwelling regions are reduced by as much as 60% in a 0.5° resolution of the atmospheric model of CCSM3.5 compared to a 2.0° horizontal resolution version of the atmospheric model. There are also significant differences in the SST biases. In the Southern Ocean, a warm SST bias dominates in CCSM3/HYCOM simulations whereas there are cold SST biases in CCSM3/POP runs. Also, the cold SST bias in the Northern Atlantic is larger in CCSM3/HYCOM simulations than in CCSM3/POP simulations.

Figure 2 shows a comparison of the biases of SSS in CCSM3/HYCOM and CCSM3/POP simulations. We see similar spatial patterns of SSS biases in tropical oceans in both model configurations. The negative SSS biases in the Atlantic and the positive SSS biases in the Northern Pacific are also similar in the CCSM3/HYCOM and CCSM3/POP simulations. However, CCSM-HYCOM2 is uniformly more saline in the Northern Pacific Ocean whereas CCSM-POP exhibits a meridional gradient with positive and negative biases. Furthermore, the SSS biases are different over the Atlantic sector of the Arctic Ocean.

Large and Danbasoglu (2006) analyzed the upper-ocean biases in the CCSM3. To understand the sources of the biases (Figs.1 and 2) in CCSM3/HYCOM simulation, we also perform a series of model experiments with perturbed parameters, including Smagorinsky viscosity and along-isopycnal and vertical diffusivities in HYCOM2 (not shown). It is found that although a reduction of the Smagorinsky viscosity parameter from 0.2 to 0.1 does not strengthen the Atlantic Meridional Overturning Circulation (AMOC), it reduces the biases in the Equatorial Undercurrent (EUC) and improves the simulation of climate variability in the tropical Pacific. The increase in isopycnal eddy diffusivity greatly reduces the cold and fresh biases in the North Atlantic, but slightly worsens the warm bias in the Southern Ocean. CCSM3/HYCOM employs KPP (Large et al. 1994) as the standard vertical diffusivity scheme. The increase in background diffusivity leads to a stronger AMOC and a great reduction of the cold bias in the North Atlantic, but it is detrimental to the SSS in the Arctic. This shows that the model biases cannot be reduced simply by "tuning" model parameters and that the changes in representation of physical processes have non-local effects on the coupled simulation, consistent with the findings of Large and Danabasoglu (2006). The relevant mechanism for these observed changes is unclear so far in the comparison of the mean climate from the model simulations. In the following section we will turn our attention to the modes of climate variability, which may provide a different perspective on the performance of coupled model simulation.

3 Atmospheric Modes

3.1 Annular Modes

The annular modes are associated with the interaction of atmospheric jets and high-frequency synoptic eddies. The red-noise variation of surface wind stress, precipitation, and surface heat fluxes associated with the atmospheric annular modes form a suite of forcings to the ocean circulation and its long-term variability (e.g. Liu 2011). The systematic errors in the strength and the position of the annular modes may be caused by the model's mean climate due to model resolution, numerics, and physics; however, these issues could also potentially cause bias in the long-term climate variability. This in turn can feedback into the mean climate through the eddy-mean flow interaction facilitated by the coupling between the atmosphere and the ocean. The underlying physical mechanism of the annular modes involves the relatively fast processes in the atmosphere such as the dynamics of Hadley circulation and mid-latitude eddies and more generally the meridional mass circulation in the atmosphere (e.g. Cai and Ren 2007). Therefore, the comparison of the model annular modes with observation may also help us to understand the physical connection between the model biases and the representation of processes over remote regions and not necessarily limited to local physical processes.

3.1.1 Northern Annular Mode (NAM)

Figure 3a depicts the first empirical orthogonal function (EOF1) of sea level pressure (SLP) over 20°N-90°N for a northern cold half year (October-March) in CCSM3/HYCOM. The pattern represents the Northern Annular Mode (NAM, Thompson and Wallace 2000) and explains 36.5% of the total variance in SLP. Figures 1b-d show the regressions of surface wind stress, precipitation, and surface temperature on the corresponding principal component of EOF1 in Fig. 1 (NAM). To make the quantitative comparison of the modes between models and the observations convenient, the EOF patterns and regressions in Fig. 3 and the following figures are all normalized by the standard deviation of the corresponding EOF modes. Figures 4 and 5 are the counterparts of Fig. 3 for the CCSM3/POP simulation (which explains 31.6% of the total SLP variance) and for the NCEP/NCAR reanalysis from 1951 to 2010 (which explains 29.6%

of the total SLP variance). The surface wind stress is replaced by the near-surface wind (at the level $\sigma = 0.995$) in Fig. 5b for the NCEP/NCAR reanalysis because of data unavailability.

In general terms, the modeled NAM patterns in both CCSM3/HYCOM and CCSM3/POP are similar to those in Thompson and Wallace (1998) and in Fig. 5a, which is based on the NCEP/NCAR reanalysis. The positive phase of NAM is associated with a stronger polar vortex and less polar air mass (low SLP), and stronger zonal westerly jets over 55°N-65°N while the westerly jets over 35°N-45°N are weakened. Accordingly the storm tracks over the North Pacific (NP) and North Atlantic move poleward with enhanced precipitation over 55°N-65°N and decreased precipitation over 35°N-45°N (Figs. 3-5c). The prevailing surface temperature anomaly pattern associated with positive NAM is warmer conditions over the Euro-Asian continent and southern North America, and colder conditions over the Arctic, Alaska, Canada, and Greenland (Figs. 3-5d).

Important differences exist, however, among the NAM patterns in the two model simulations and in observations. The intensity of the anomalous SLP center over the NP of positive NAM in both model simulations (Figs. 3-4a) is comparable to the center over the North Atlantic. The NCEP/NCAR reanalysis, however, depicts the anomalous North Pacific SLP center (Fig. 5a) with weaker intensity and with smaller spatial extension compared to the North Atlantic SLP Center. In addition the precipitation patterns over the NP in both models are consistently stronger than those in the NCEP/NCAR reanalysis, though we note that the precipitation in the reanalysis may contain uncertainty compared to the actual precipitation.

Over the North Atlantic sector, the location of the anomalous SLP center associated with the NAM in both models is biased to the east of the center in the observation. This leads to systematic biases in the location of the corresponding anomalous surface wind stress and precipitation, both of which are important forcings to the AMOC. In the observation we can see the poleward surface wind anomaly over the Northwestern Atlantic and along the east coast of North America (Fig. 5b). The corresponding precipitation anomalies are located over south of Greenland and over the Labrador Sea (Fig. 5c) where the deep ocean convection is essential to the AMOC. It is possible that the systematic errors in the positions of the NAM SLP centers are influencing the SST and SSS biases (Figs. 1 and 2). This is because the NAM variability is directly related to the synoptic eddies, which provide the random (red-noise) momentum and fresh-water forcing to dictate the mean and the variability of the ocean circulation. This can be seen in the comparison of regression of the lower-tropospheric (at lowest model level) eddy kinetic energy (EKE) on NAM in CCSM3/HYCOM with that in the observations. On the basis of the available model output, the EKE is defined as

$$EKE = \frac{1}{2}[\overline{(u^2 + v^2)} - (\overline{u}^2 + \overline{v}^2)] \tag{1}$$

where the overbar — denotes the monthly mean. The EKE anomalies associated with the NAM in the NP and the North Atlantic in CCSM3/HYCOM are located on the east side of the ocean basin (Fig. 6a) whereas in the observation (Fig. 6b) the EKE center over the NP extends from the Kuroshio extension eastward into the northeast Pacific, and the (negative) EKE center over the North Atlantic extends into the Labrador Sea. Figure 6, together with regressions of surface wind stress and precipitation in earlier figures, suggests that there are systematic biases in the spatial structure of synoptic eddies and therefore momentum and fresh water forcing, which could potentially contribute to the bias in the mean climate and its variability.

Although the existence and dynamics of the NAM could largely be attributed to the interaction of zonal jets and synoptic eddies, theoretical and observational studies also suggest the role of tropical diabatic heating and meridional mass circulation on the variability of the NAM (e.g. Cai and Ren 2007). Here we further check the relationship of the NAM and tropical precipitation, a proxy for tropical diabatic heating, in model simulations and observations. Figures 3-5c show that the positive phase of the NAM in both model simulations and observations is associated with increased precipitation and diabatic heating over the central tropical Pacific in the Northern Hemisphere. The spurious, large negative precipitation anomalies in the equatorial Pacific in the CCSM3/POP simulation may be due to the double ITCZ bias in the CCSM3 model. The tropical precipitation pattern associated with the NAM in CCSM3/HYCOM (Fig. 3c) is closer to the observation (Fig. 5c). From the regressions of precipitation (Figs. 3-5c) and near-surface temperature (Figs. 3-5d) on the NAM, we can see that neither the observation nor either of the model simulations suggests the direct linkage between ENSO and the NAM, consistent with the results of L'Heureux and Thompson (2006).

3.1.2 Southern Annular Mode (SAM)

The SAM is the leading mode of the mid-high latitude general circulation over the Southern Hemisphere (Thompson and Wallace 2000). Figures 7-9 show the structures of the SAM, which is represented by the first EOF (EOF1) of sea level pressure over 20°S-

90°S (Figs. 7-9a) from April through September and regressions of surface wind stress (Figs. 7-8b) or surface wind (Fig. 9b), precipitation (Figs. 7-9c), and surface temperature (Figs. 7-9d) upon the principal component (PC) of the EOF1 of sea level pressure, in CCSM3/HYCOM, CCSM3/POP, and in the NCEP/NCAR reanalysis. The EOF1 of sea level pressure explains 40% of the total variance in the CCSM3/HYCOM simulation and 35.5% in CCSM3/POP, and both are higher than the 28.5% in the NCEP/NCAR reanalysis.

Although the general features of the SAM are similar in the model simulations and in the reanalysis data, the modeled SAM in CCSM3/HYCOM is more zonally distributed than in CCSM3/POP and in the reanalysis data. Consistent with the findings of L'Heureux and Thompson (2006), a stationary Rossby wave train exists in the SAM in the reanalysis data (Fig. 9a) and may be related to the convective heating over the western Pacific. The wavy character of the SAM signal is relatively weak in the model simulations, particularly in the CCSM3/HYCOM simulation. Furthermore, the associated surface wind stress in CCSM3/HYCOM is much weaker than that in the CCSM3/POP simulation. The SAM-related precipitation anomalies in the mid-latitudes in both simulations are similar. The positive phase of the SAM is associated with a cooler Antarctic surface temperature (Figs. 7-9d), but with a warmer Antarctic Peninsula in both CCSM3/POP and the reanalysis data.

The associated tropical precipitation anomaly in the reanalysis data (Fig. 9c) resembles the pattern of ENSO, i.e. enhanced precipitation over the mid-equatorial Pacific and reduced precipitation over the mean ITCZ and SPCZ zones, also consistent with the analysis of L'Heureux and Thompson (2006). We do not observe a similar relationship in the CCSM3/POP simulation, possibly because of the spurious double ITCZ issue in the simulation. The SAM-tropical-precipitation teleconnection in CCSM3/HYCOM seems more organized and closer to the relationship in reanalysis, though the enhanced precipitation anomaly is farther to the south of the equatorial Pacific (Fig. 7c).

3.2 Pacific-North-American (PNA) Pattern

The PNA pattern is usually represented by the correlation or EOF pattern of 500-hPa geo-potential height (Wallace and Gutzler 1981), but it is also apparent in the second EOF of the winter or the October-March SLP (Fig. 10.15 in Wallace and Hobbs 2006). Here we use the second EOF of SLP to represent the PNA pattern. The comparison of the PNA patterns in CCSM3/HYCOM (Fig. 10a, 15.7% of the total variance), CCSM3/POP (Fig. 11a, 15.9% of the total variance) simulations with the reanalysis data (Fig. 12a, 14.5% of the total variance), and the regressions of surface wind or wind stress, precipitation, and surface temperature on the PNA pattern are further explained below.

Although the details differ, the negative SLP center over the NP associated with the positive phase of the PNA pattern is very similar in the model simulations and in the reanalysis data (Figs. 10-12a). The corresponding wind (Figs. 10-12b) and precipitation (Figs. 10-12c) anomalies over the NP and the surface temperature anomalies over the Eurasian and the North American continents (Fig. 10-12d) are also similar.

However, there are important differences in the dynamical nature of the seemingly similar PNA patterns between the CCSM3/HYCOM simulation on one side and the CCSM3/POP simulation and the reanalysis data on the other side. In both CCSM3/POP (Fig. 11c-d) and the reanalysis data (Fig. 12c-d), the precipitation and surface temperature anomalies over the tropical Pacific associated with the PNA resemble the warm ENSO anomalies, whereas the same relationship between the ENSO and the PNA does not exist in the CCSM3/HYCOM simulation. In fact, the correlations between the EOF1 of SST in the tropical Pacific from October through March (i.e. the ENSO signal) and the PNA pattern is 0.56 in the CCSM3/POP simulation (200-year data) and 0.51 in the detrended reanalysis data (1949-2008). However, the correlation between the EOF1 of the tropical Pacific SST and the PNA is only -0.05 in CCSM3/HYCOM. The disappearance of a PNA-ENSO correlation may be related to the ENSO signal in the total variance of the tropical Pacific SST being much weaker in the CCSM3/HYCOM simulation as described by Michael et al. (2012) in a companion paper. Although the CCSM3/HYCOM simulation is far from the observation in terms of the ENSO-PNA relationship, the existence of the PNA pattern in CCSM3/HYCOM supports the idea that the PNA pattern could be a pattern of internal variability (Straus and Shukla 2002), rather than a pattern forced by the tropical SST anomalies.

The only difference in the two simulations is in the ocean model configurations in vertical coordinates and associated parameterization of physical processes. The difference in the modeled atmospheric modes shows that these atmospheric modes are highly sensitive to the representation of ocean processes in the coupled model, but so far the mechanism responsible for the difference is not clear and needs more careful research with more and well-designed experiments.

4 SST modes

4.1 Atlantic SST

Here we compare the SST variability over the North Atlantic by conducting EOF decomposition for the averaged October-March SST over 0°-60°N in both model simulations and detrended SST observations based on the latest version of the Extended Reconstructed Sea Surface Temperature (ERSST, Smith et al. 2008). The SST modes based on the cold half year (October-March) are almost the same as the modes based on annual mean SST in the observations (Delworth et al. 2007) and also in our model simulations (not shown).

The EOF1 of the North Atlantic SST represents the Atlantic Multidecadal Variability (e.g. Liu 2011) or the Atlantic Multidecadal Oscillation (AMO, Schlesinger and Ramankutty 1994; Delwoth et al. 2007). The time series of the AMO in the latest version of ERSST (Smith et al. 2008) from 1949 to 2008 in Fig. 13c (also in Delworth et al. 2007) shows that the period of the AMO is about 60 years, while the time series of the AMO in the CCSM3/HYCOM (Fig. 13a) and CCSM3/POP simulations (Fig. 13b) show the AMO has no fixed period (note that the years in Figs. 13a,b are virtual).

However, the spatial structures of the AMO in the model simulations (Fig. 14 for CCSM3/HYCOM and Fig. 15 for CCSM3/POP) show significant differences from the AMO in the observation (Fig. 16). In the observation, the SST pattern (Fig 16a) shows anomalies of the same sign across the North Atlantic, with two maximum centers in the subpolar gyre and the east tropical Atlantic and one minimum center extending eastward from the west boundary of the subtropical Atlantic (e.g. Delworth et al. 2007). Associated with this SST pattern are a weakened mid-latitude westerly around 45°N and an enhanced westerly anomaly and cross-equatorial wind in the tropical Atlantic (Fig. 16b), enhanced ITCZ precipitation (Fig. 16c), and a dipole SLP anomaly with an anti-cyclonic anomaly over Greenland and the subpolar Atlantic and a cyclonic anomaly over the subtropical Atlantic (Fig. 16d).

In CCSM3/HYCOM, the EOF1 of Atlantic SST is confined in the subpolar area, i.e. mainly the high SST anomaly south of Greenland including over the Labrador Sea (Fig. 14a). Although the location of the anti-cyclonic center over Greenland is close to the location in the observation, the cyclonic center has a bias to the east and is close to Europe (Fig. 14d). The anomalous circulation (Fig. 14b,d) is characterized by a weakened zonal jet over 50-70°N and an enhanced westerly around 30°N. The EOF1 of the Atlantic SST in the CCSM3/POP simulation (Fig. 15a) is the subpolar warm center located east of the one in observation. The anomalous anti-cyclonic center in the SLP (Fig. 15d) also has an eastward bias and is much weaker compared to the center in the observation. Therefore, despite the verifying multidecadal time period of the AMO in the coupled model simulations, the phenomena as characterized by AMO's spatial variations and teleconnections and the underlying mechanism are likely different from those of the observed AMO.

The centers for modeled AMO variability are also where the SST biases over the North Atlantic are largest in the models (Fig. 1). This suggests that the biases in the simulation of the AMO may be related to the biases in the location of the atmospheric jets, storm tracks, and the shift of, or structural changes in, the high and low SLP centers. For example, we have seen from Fig. 16d that the anti-cyclonic center over Greenland in the observation causes southward surface wind stress in the east Greenland Sea and easterly wind stress along the southern tip of the Greenland Island towards the Labrador Sea. The wind stress in the subpolar Atlantic is mainly a zonal easterly anomaly in the

CCSM3/HYCOM simulation and a westerly anomaly in the CCSM3/POP simulation. Another example is the near surface (atmospheric) EKE, as defined by Eq. (1), associated with AMO in observation and in model simulation (Fig. 17, data from CCSM3/POP are not available). In the CCSM3/HYCOM simulation, the eddy activity, represented by the regression of the EKE upon the AMO, is decreased over the subpolar Atlantic and increased over the subtropical Atlantic (Fig.17a). The regression of the EKE in reanalysis data (Fig. 17b) has a more complicated structure over the subpolar Atlantic region, and possibly reflects the complexity in air-sea-ice-topography interaction in the region, though some of the fine structure might be related to the uncertainty in reanalysis data.

4.2 The Southern Ocean SST

Figures 18-20a show the EOF1 of the SST of the Southern Ocean (south of 40°S) averaged over the austral winter months (April-September) for CCSM3/HYCOM (Fig. 18, 22% of the total variance), CCSM3/POP (Fig. 19, 19.8% of the total variance), and ERSST (Fig. 20, 16.7% of the total variance). The other panels in Figs. 18-20 show linear regressions of surface wind stress or wind, precipitation, and SLP upon the principal component of the EOF1 of the SST. The EOF1 of the Southern Ocean SST in CCSM3/HYCOM simulations is mainly a zonal mode with the SST seesawing between the subpolar and midlatitudinal oceans. The surface wind stress associated with the mode is characterized by the enhanced westerly over 50-70°S (Fig. 18b), and the SLP pattern in the Pacific sector resembles the SAM mode. Note that the bias in the SST over the Southern Ocean in CCSM3/HYCOM in Fig. 1 is also mainly a zonal mode. The EOF1 of the Southern Ocean SST in CCSM3/POP simulations is mainly the SST seesawing between the Ross Sea and Weddell Sea. The surface wind stress associated with the mode is characterized by the enhanced westerly over 50-70°S (Fig. 19b) as in the CCSM3/HYCOM simulation, but it has a more apparent wavy structure, which is also seen in the SLP pattern as a Rossby wave train originating from south Australia (Fig.19d).

The Rossby wave structure is more clearly shown in the Pacific sector of the EOF1 of the observed ERSST data over the Southern Ocean (Fig. 20a) and the associated surface wind (Fig. 20b) and SLP (Fig. 20d). Figure 20 suggests that the observed SST mode in the Southern Ocean and associated anomalous circulation is closely related to the (negative phase of) ENSO in the tropical Pacific. The correlation between the ENSO and the PC of the EOF1 of the Southern Ocean SST is -0.66 in ERSST data for 1949-2008. The correlations between ENSO and the EOF1 of the Southern Ocean SST in both model simulations are also significant; both are -0.33 with 200-year data. The spatial patterns of the first Southern Ocean SST mode in the two model simulations (Figs. 18a and 19a) show a large deviation from the observed pattern in Fig. 20a. We also observe the differences of the regression of precipitation upon the SST mode (Fig. 18-20c): The precipitation anomalies in the tropics resemble the La Niña pattern. However, both model simulations (Fig. 18-19c) show a large deviation from the observed pattern (Fig. 20c).

Figures 18-20 and the correlation between ENSO and the SST in the Southern Ocean suggest that the biases in the simulated Southern Ocean SST mode in the models may be related to the biases in the simulation of ENSO in the tropics, in addition to the poor representation of local physical processes. This non-local linkage between the tropics and the Southern Ocean may be a two-way interaction. The difference in the model simulations reflects the role of different ocean model configurations, but at this stage we still do not know the mechanism responsible for the difference shown in the comparison.

5 Summary and Conclusions

The latest version of the Hybrid Coordinate Ocean Model (HYCOM2.2) is incorporated into the CCSM3 framework to increase the structural diversity of the ocean component in the CCSM framework. In this paper, we compare the differences in mean climate and modes of climate variability in the simulations using two different ocean models under the same CCSM3 framework. The simulations are conducted by using the standard present-day (1990) climate forcing. To gain some understanding of the model biases we conduct a detailed comparison of the Northern and Southern annular modes (NAM and SAM), the Pacific-North-American (PNA) teleconnection pattern, the Atlantic Multi-decadal Oscillation (AMO), and the main Southern Ocean SST mode in the model simulations and the observations (NCAR/NCEP reanalysis data and the latest version of the ERSST data). The following conclusions are drawn from the present study.

(1) The SST biases in the CCSM3/HYCOM simulation in the major upwelling regions are similar to that in CCSM3/POP, which are believed to be at least partly related to the resolution of the coupled model (Gent et al. 2010). The cold bias in the North Atlantic is larger in CCSM3/HYCOM than in CCSM3/POP, and the pattern of Southern Ocean SST biases is mostly warm in CCSM3/HYCOM and cold in CCSM3/POP.

(2) The dominant mode in mid-to-high latitudes in the Northern Hemisphere in both simulations is the Northern Annular Mode (NAM), and the structure is similar to the structure of the mode in the observations. However, the SLP centers associated with the

NAM over the North Atlantic in both simulations are shifted to the east relative to the observations. These systematic errors are associated with the systematic shift of the atmospheric jets and storm tracks (eddy activity). We suggest that the systematic shift of the NAM center may be related to the mean SST biases in the North Atlantic through interaction between the mean flow and the synoptic eddies.

(3) The dominant mode in mid-to-high latitudes in the Southern Hemisphere in both simulations is the Southern Annular Mode (SAM), and the structure in the CCSM3/POP simulation is similar to the structure of the mode in the observation. The SAM in CCSM3/HYCOM is more zonal and lacks the observed wavy pattern. Both modeled SAM patterns show a relationship with anomalous precipitation in the tropical Pacific.

(4) Although in both simulations the second mode for the circulation over mid-to-high latitudes is the PNA pattern, the dynamics of the PNA are different in the model simulations. The PNA pattern in CCSM3/HYCOM shows no relationship with the ENSO in the tropics, and its generation in the model is attributed to the internal variability as suggested by Straus and Shukla (2002). The PNA patterns in the CCSM3/POP simulation and observations are forced patterns with high correlation with the ENSO index in the tropical Pacific (Wallace and Gutzler 1981).

(5) The Atlantic Multidecadal Oscillation (AMO) patterns in both simulations show large biases from the observation in both the spatial structure and time scales. The main centers of the AMO in model simulations are confined to the subpolar Atlantic, and

the regressed atmospheric eddy structure in the model simulations seems over simplified compared to the observed structure.

(6) The comparison of the dominant mode of the Southern Ocean SST and its relationship with ENSO shows that the bias of the Southern Ocean SST variability in both the simulations partly originate from tropical bias, in addition to the misrepresentation of local physical processes.

Given the same configurations of atmospheric, ice, and land-surface models, the differences mentioned above highlight the importance of ocean model configuration in coupled climate simulations. In Part II, Michael et al. (2012) discuss in detail the differences of the ENSO simulation in the two models. It is found that that the erroneously strong biennial variability of the eastern equatorial Pacific SST present in CCSM3/POP is substantially reduced in CCSM3/HYCOM. The role of ocean model configuration in model simulations is non-local and far-reaching through the effects of model configuration on the coupled modes of climate variability. However, we still lack effective diagnostic tools to reveal the connection between the physical processes and these modes in climate models. This hinders us from fully understanding what causes the difference in model simulations and what causes the model biases. However, it is important to understand the effect of numerical choices in vertical coordinates in the performance of earth system modeling. We are in the process of coupling HYCOM with the latest versions of CCSM (CCSM4) and CESM as well as developing new methods to better understand and reduce model biases.

Acknowledgments The research was supported by DOE grant DE-FG02-07ER64470. We also thank W. G. Large, N. Norton, A. Wallcraft, S. Yeager, and NCAR’s Ocean Modeling Working Group for their support and for their assistance with incorporating the HYCOM into the CCSM. We acknowledge the Program for Climate Model Diagnosis and Intercomparison (PCMDI) and the WCRP's Working Group on Coupled Modelling (WGCM) for their roles in making available the CCSM3 present-day control experiment data under the WCRP CMIP3 multimodel dataset. Support of this dataset is provided by the Office of Science, U.S. Department of Energy.

References

Bleck R (2002) An oceanic general circulation model framed in hybrid isopycnic-Cartesian coordinates. Ocean Modelling 4:55-88

Cai M, R-C Ren (2007) Meridional and Downward Propagation of Atmospheric Circulation Anomalies. Part I: Northern Hemisphere Cold Season Variability. J Atmos Sci 64:1880–1901

Chassignet EP, LT Smith, GR Halliwell, R Bleck (2003), North Atlantic simulation with the HYbrid Coordinate Ocean Model (HYCOM): Impact of the vertical coordinate choice, reference density, and thermobaricity. *J Phys Oceanogr* 33: 2504-2526

Chassignet EP (2011) Isopycnic and hybrid ocean modeling in the context of GODAE. In *Operational Oceanography in the 21st Century* [Schiller A and G Brassington, Eds.], Springer, 263-294

Chen CC, PJ Rasch (2011) Climate Simulations with an Isentropic Finite Volume Dynamical Core. J Clim doi:10.1175/2011JCLI4184.1 (in press)

Collins WD, CM Bitz, ML Blackmon, et al (2006) The Community Climate System Model Version 3 (CCSM3). J Clim 19: 2122-2143

Danabasoglu G, WG Large, JJ Tribbia, et al (2006) Diurnal coupling in the tropical oceans of CCSM3. J Clim 19: 2347:2365

Danabasoglu G, R Ferrari, JC McWilliams (2008) Sensitivity of an Ocean General Circulation Model to a Parameterization of Near-Surface Eddy Fluxes. J Clim 21: 1192–1208

Danabasoglu G, SC Bates, BP Briegleb, et al (2011) The CCSM4 Ocean Component. J Clim doi: 10.1175/JCLI-D-11-00091.1 (in press)

Delworth T, R Zhang, M Mann (2007) Decadal to centennial variability of the Atlantic from observations and models. In *Ocean Circulation: Mechanisms and Impacts, Geophysical Monograph Series 173*, Washington, DC, American Geophysical Union, 131-148

Gent PR, SG Yeager, RB Neale, et al (2010) Improvements in a half degree atmosphere/land version of the CCSM. Clim Dyn 34:819-833

Gent PR, G Danabasoglu, LJ Donner, et al (2011) The Community Climate System

Model Version 4. J Clim 24: 4973-4991

Griffies SM, A Biastoch, C Böning et al (2009) Coordinated Ocean-ice Reference Experiments (COREs), Ocean Modelling, 26:1-46

Jablonowski C, DL Williamson (2006) A Baroclinic Instability Test Case for Atmospheric Model Dynamical Cores, Q J Roy Met Soc132: 2943-2975

Large WG, JC McWilliams, SC Doney (1994) Oceanic vertical mixing: A review and a model with a nonlocal boundary layer parameterization. Rev Geophys 32:363–403

Large WG, G Danabasoglu (2006) Attribution and Impacts of upper-ocean biases in CCSM3. J Clim 2325-2346

L'Heureux ML, DWJ Thompson (2006) Observed Relationships between the El Niño–Southern Oscillation and the Extratropical Zonal-Mean Circulation. J Clim 19:276–287

Liu Z (2011) Dynamics of Interdecadal Climate Variability: An Historical Perspective. J Clim doi: 10.1175/2011JCLI3980.1 (in press)

McAvaney BJ, C Covey, S Joussaume, et al (2001) Model Evaluation. In: *Climate Change 2001: The Scientific Basis. Contribution of Working Group I to the Third Assessment Report of the Intergovernmental Panel on Climate Change* [Houghton JT, Y Ding et al (eds.)], Cambridge University Press, Cambridge, United Kingdom and New York, NY, USA. 471-523

Michael JP, V Misra, EP Chassignet, et al (2012) Comparison of HYCOM2 and POP Models in the CCSM3.0 Framework. Part II : ENSO fidelity. Submitted to Clim Dyn

Neale RB, JH Richter, M Jochum(2008) The impact of convection on ENSO: from a delayed oscillator to a series of events. J Clim 21:5904–5924

Randall DA, RA Wood, S Bony et al (2007) Climate Models and Their Evaluation. In: *Climate Change 2007: The Physical Science Basis. Contribution of Working Group I to the Fourth Assessment Report of the Intergovernmental Panel on Climate Change* [Solomon S, D Qin et al (eds.)]. Cambridge University Press, Cambridge, United Kingdom and New York, USA. 590-662

Schlesinger ME, N Ramankutty (1994) An oscillation in the global climate system of period 65–70 years. Nature 367: 723-726

Smith RD, JK Dukowicz JK, RC Malone (1992) Parallel Ocean General Circulation

Modeling. Physica D 60: 38-61

Smith TM, RW Reynolds, TC Peterson, J Lawrimore (2008) Improvements to NOAA’s Historical Merged Land–Ocean Surface Temperature Analysis (1880–2006). J Clim 21: 2283–2296

Straus DM, J Shukla (2002) Does ENSO force the PNA? J Clim 15:2340-2358

Thompson DWJ, JM Wallace (2000) Annular Modes in the Extratropical Circulation. Part I: Month-to-Month Variability. J Clim 13:1000–1016

Wallace JM, DS Gutzler (1981) Teleconnections in the geopotential height field during the Northern Hemisphere winter. Mon Wea Rev 109:784-812

Figure Captions

Figure 1. SST biases (ºC) in CCSM3/HYCOM simulations (left) and CCSM3/POP simulations (right) with T42 and T85 CAM3.

Figure 2. SSS biases (psu) in CCSM3/HYCOM simulations (left) and CCSM3/POP simulations (right) with T42 and T85 CAM3.

Figure 3. The NAM - the first EOF of the October-to-March-averaged sea level pressure (SLP) over 20°N-90°N for 200-year coupled CCSM3/HYCOM simulations with present-day forcing (a). The linear regressions of surface wind stress (b), precipitation (c), and surface temperature (d) upon the NAM. The regressions are normalized by the standard deviation of the NAM mode.

Figure 4. The same as Fig. 3, but for 200-year CCSM3/POP simulation with present-day forcing.

Figure 5. The same as Fig. 3, but with 60-year (1951-2010) NCEP/NCAR reanalysis data. The surface wind stress in panel (b) and surface temperature in (d) are replaced by wind and air temperature at the lowest model level (σ=0.995).

Figure 6. The linear regressions of EKE at lowest level upon the NAM in CCSM3/HYCOM simulation (a) and NCEP/NCAR reanalysis data (b), normalized by the standard deviation of the NAM mode. The data for CCSM3/POP simulation are not available.

Figure 7. The SAM - the first EOF of the April-to-September-averaged sea level pressure (SLP) over 20°S-90°S for 200-year coupled CCSM3/HYCOM simulations with present-day forcing (a). The linear regressions of surface wind stress (b), precipitation (c), and surface temperature (d) upon the SAM. The regressions are normalized by the standard deviation of the SAM mode.

Figure 8. The same as Fig. 7, but for 200-year CCSM3/POP simulation with present-day forcing.

Figure 9. The same as Fig. 7, but with 60-year (1951-2010) NCEP/NCAR reanalysis data. The surface wind stress in panel (b) and surface temperature in (d) are replaced by wind and air temperature at the lowest model level (σ=0.995).

Figure 10. The PNA pattern - the second EOF of the October-to-March-averaged sea level pressure (SLP) over 20°N-90°N for 200-year coupled CCSM3/HYCOM simulations with present-day forcing (a). The linear regressions of surface wind stress (b), precipitation (c), and surface temperature (d) upon the PNA. The regressions are normalized by the standard deviation of the PNA mode.

Figure 11. The same as Fig. 10, but for 200-year CCSM3/POP simulation with present-day forcing.

Figure 12. The same as Fig. 10, but with 60-year (1951-2010) NCEP/NCAR reanalysis data. The surface wind stress in panel (b) and surface temperature in (d) are replaced by wind and air temperature at the lowest model level (σ=0.995).

Figure 13. The time series of the AMO in CCSM3/HYCOM (a), CCSM3/POP simulations, and in observation (version 3 of ERSST data, Smith et al. 2008)

Figure 14. The AMO - the first EOF of the October-to-March-averaged SST over the North Atlantic (0-90°N) for 200-year coupled CCSM3/HYCOM simulations with present-day forcing (a). The linear regressions of surface wind stress (b), precipitation (c), and SLP (d) upon the AMO. The regressions are normalized by the standard deviation of the AMO mode.

Figure 15. The same as Fig. 14, but for 200-year CCSM3/POP simulation with present-day forcing.

Figure 16. The same as Fig. 14, but with 60-year (1949-2008) ERSST data (a) and NCEP/NCAR reanalysis data (b-d). The surface wind stress in panel (b) is replaced by wind at the lowest model level (σ=0.995).

Figure 17. The linear regressions of EKE at lowest level upon the AMO in CCSM3/HYCOM simulation (a) and NCEP/NCAR reanalysis data (b), normalized by the standard deviation of the AMO mode. The data for CCSM3/POP simulation are not available.

Figure 18. The first EOF of the April-to-September-averaged SST over the Southern Ocean (40°S-90°S) for 200-year coupled CCSM3/HYCOM simulations with present-day forcing (a). The linear regressions of surface wind stress (b), precipitation (c), and SLP (d) upon the SST mode. The regressions are normalized by the standard deviation of the SST mode.

Figure 19. The same as Fig. 18, but for 200-year CCSM3/POP simulation with present-day forcing.

Figure 20. The same as Fig. 18, but with 60-year (1949-2008) ERSST data (a) and NCEP/NCAR reanalysis data (b-d). The surface wind stress in panel (b) is replaced by wind at the lowest model level (σ=0.995).

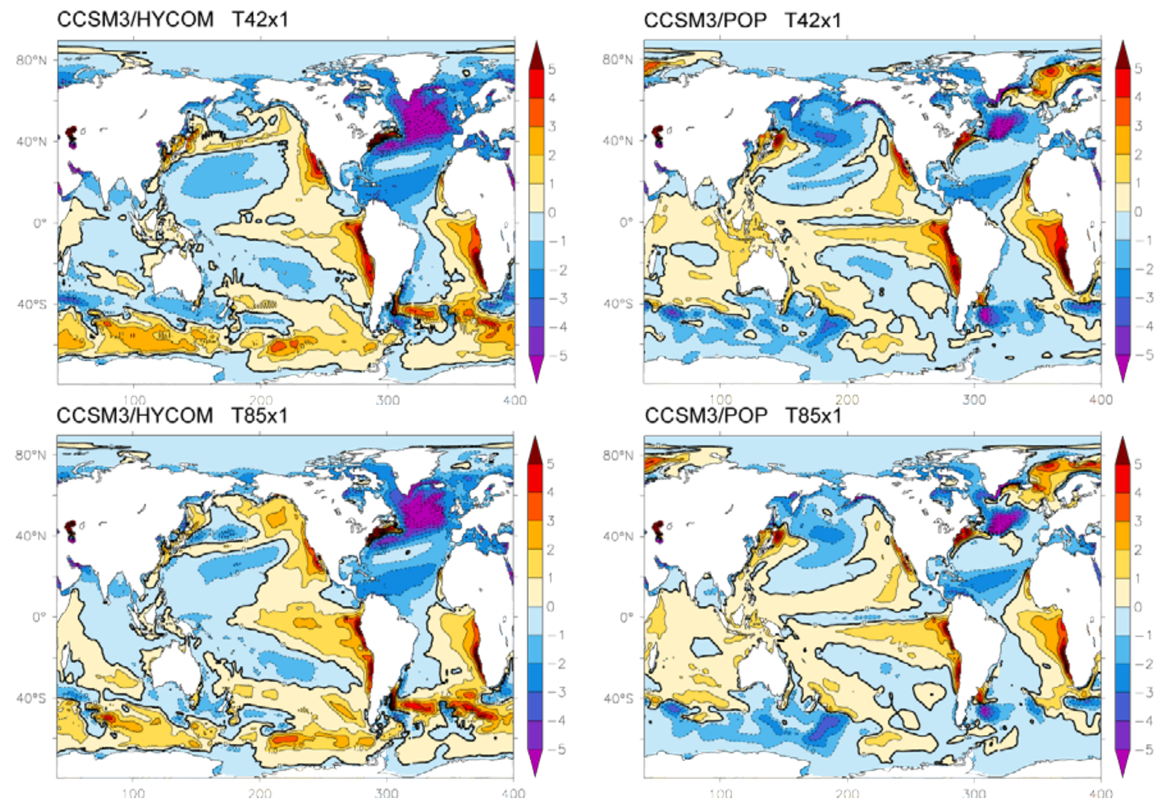

Figure 1. SST biases (ºC) in CCSM3/HYCOM simulations (left) and CCSM3/POP simulations (right) with T42 and T85 CAM3.

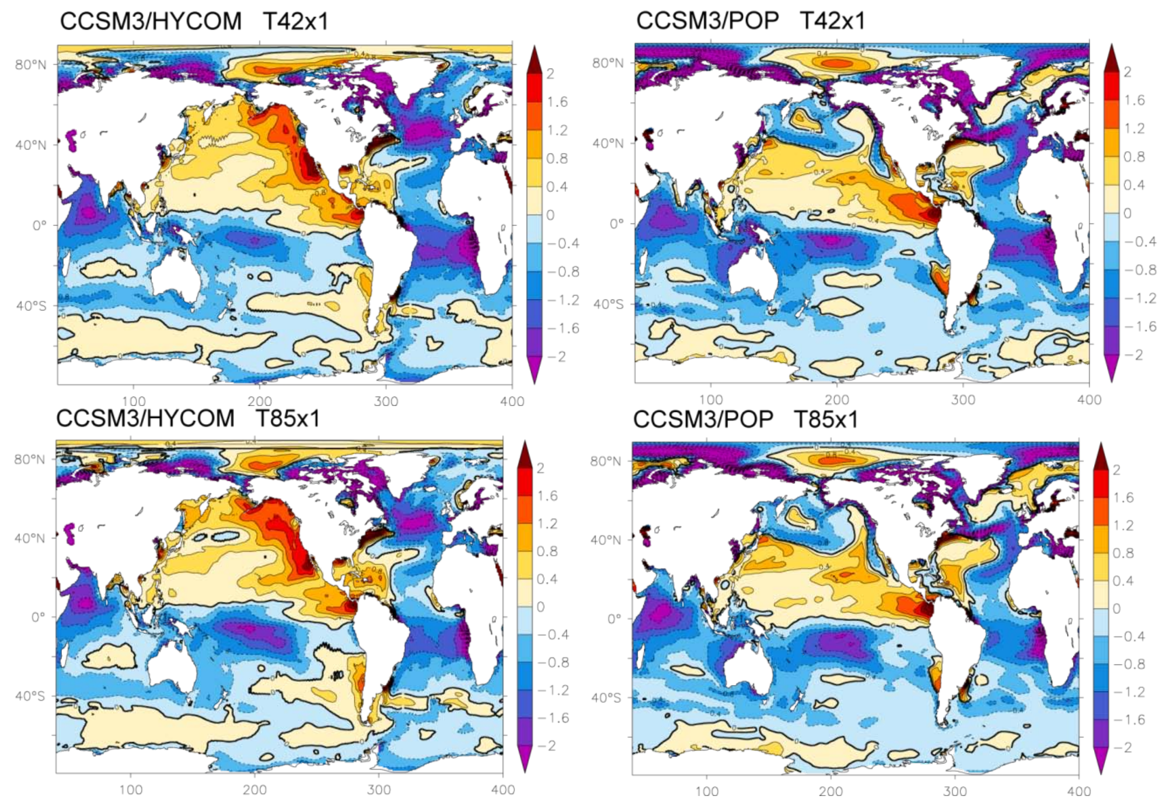

Figure 2. SSS bias (psu) in CCSM3/HYCOM simulations (left) and CCSM3/POP simulations (right) with T42 and T85 CAM3.

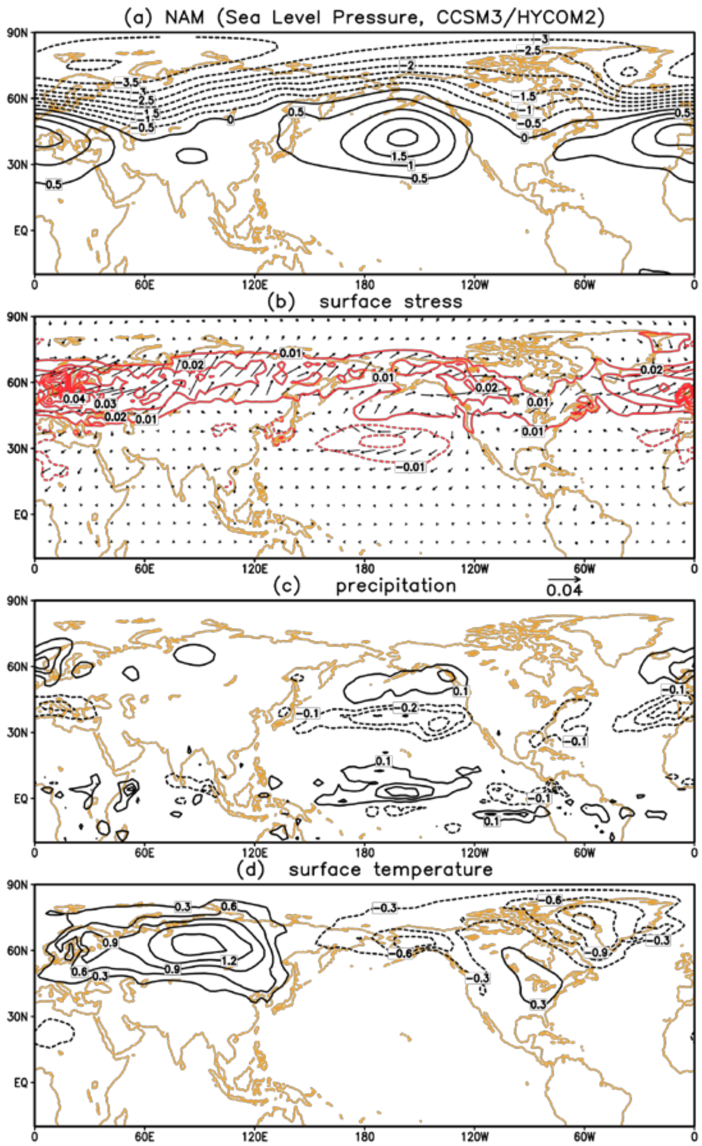

Figure 3. The NAM - the first EOF of the October-to-March-averaged sea level pressure (SLP) over 20°N-90°N for 200-year coupled CCSM3/HYCOM simulations with present-day forcing(a). The linear regressions of surface wind stress (b), precipitation (c), and surface temperature (d) on the NAM. The regressions are normalized by the standard deviation of the NAM mode.

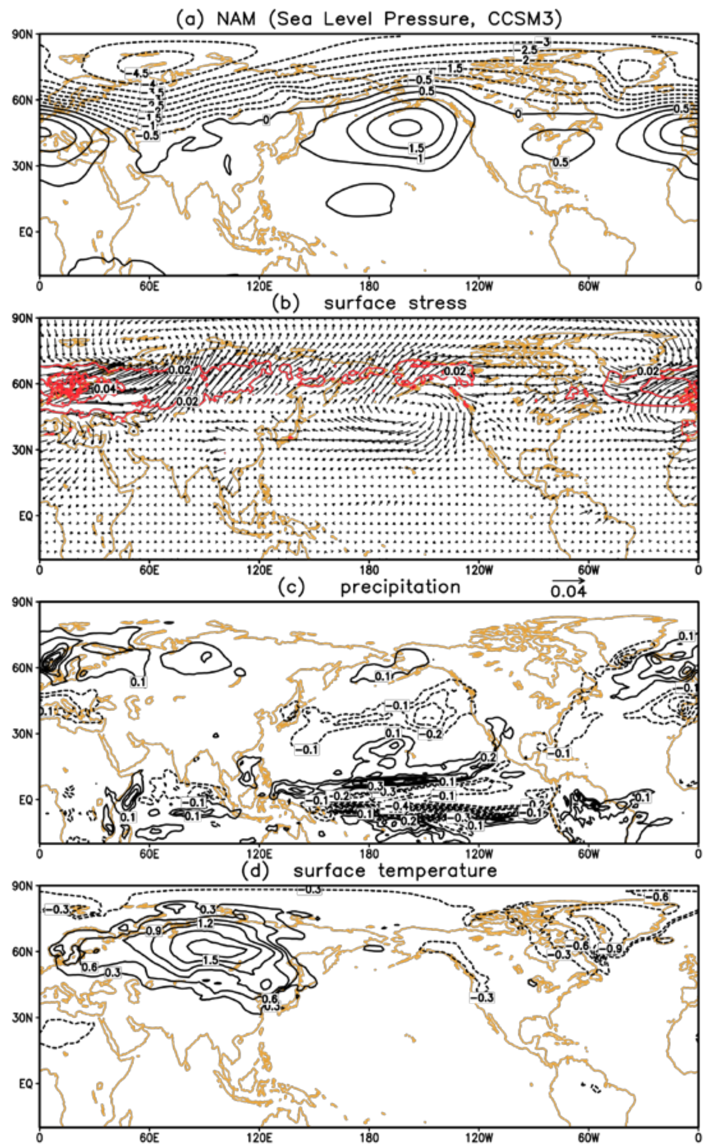

Figure 4. The same as Fig. 3, but for 200-year CCSM3/POP simulation with present-day forcing.

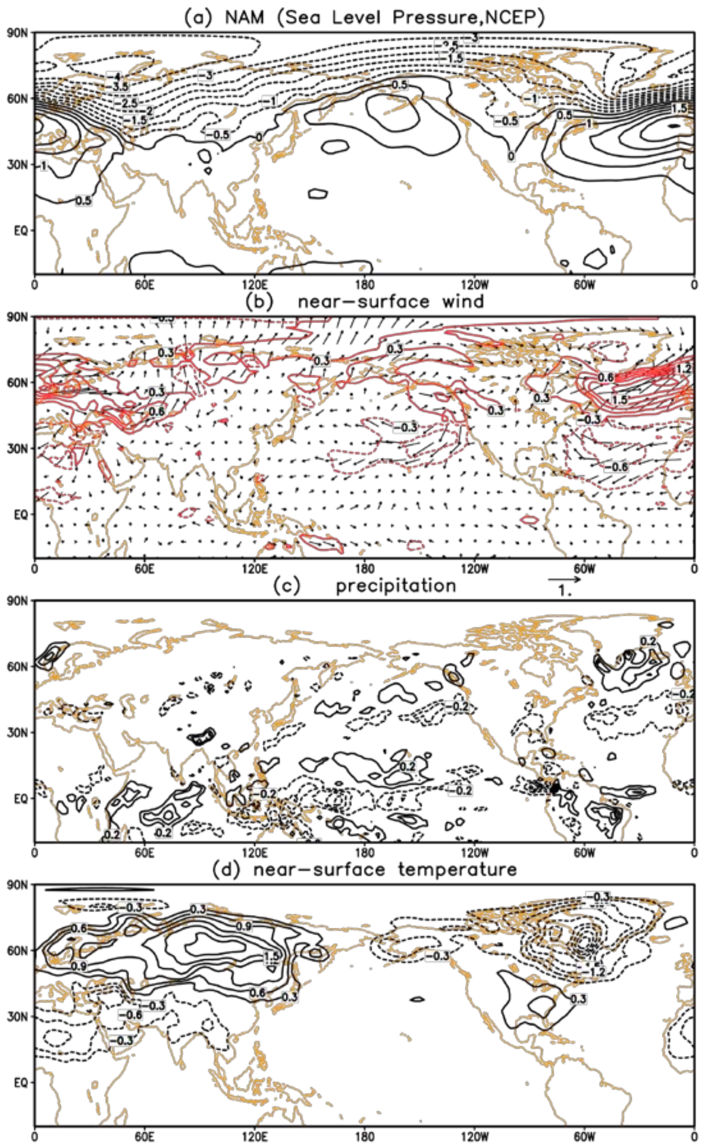

Figure 5. The same as Fig. 3, but with 60-year (1951-2010) NCEP/NCAR reanalysis data. The surface wind stress in panel (b) and surface temperature in (d) are replaced by wind and air-temperature at the lowest model level (σ=0.995).

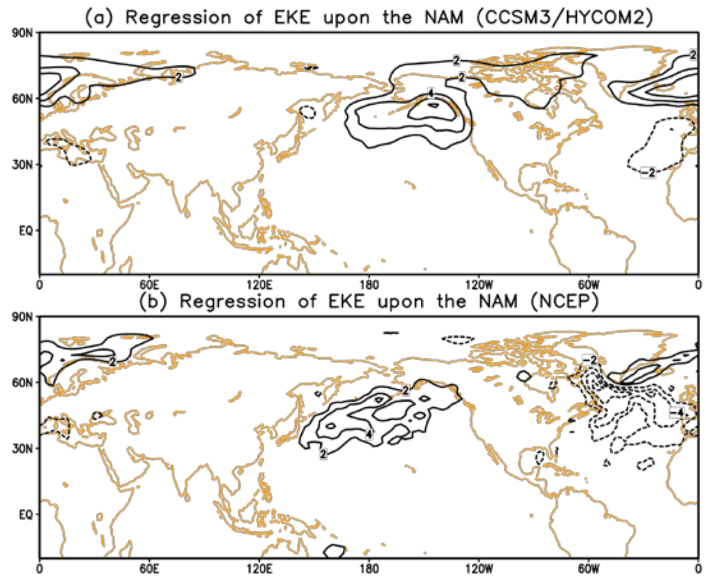

Figure 6. The linear regressions of EKE at lowest level on the NAM in CCSM3/HYCOM simulation (a) and NCEP/NCAR reanalysis data (b), normalized by the standard deviation of the NAM mode. The data for CCSM3/POP simulation are not available.

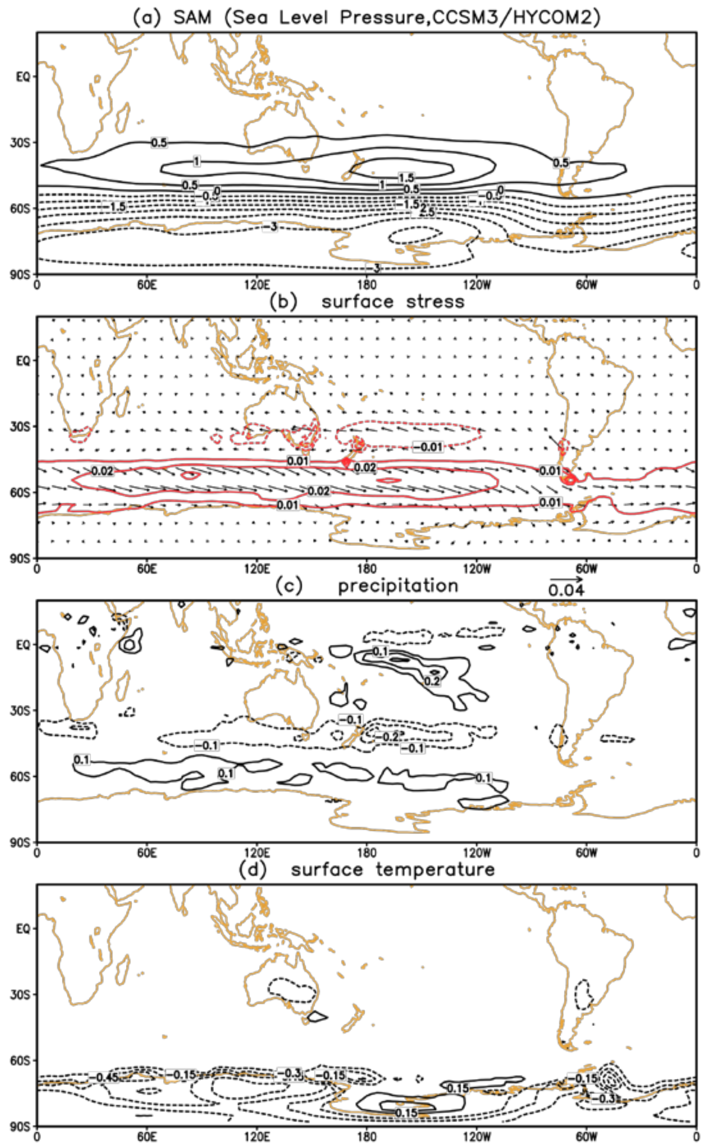

Figure 7. The SAM - the first EOF of the April-to-September-averaged sea level pressure (SLP) over 20°S-90°S for 200-year coupled CCSM3/HYCOM simulations with present-day forcing (a). The linear regressions of surface wind stress (b), precipitation (c), and surface temperature (d) upon the SAM. The regressions are normalized by the standard deviation of the SAM mode.

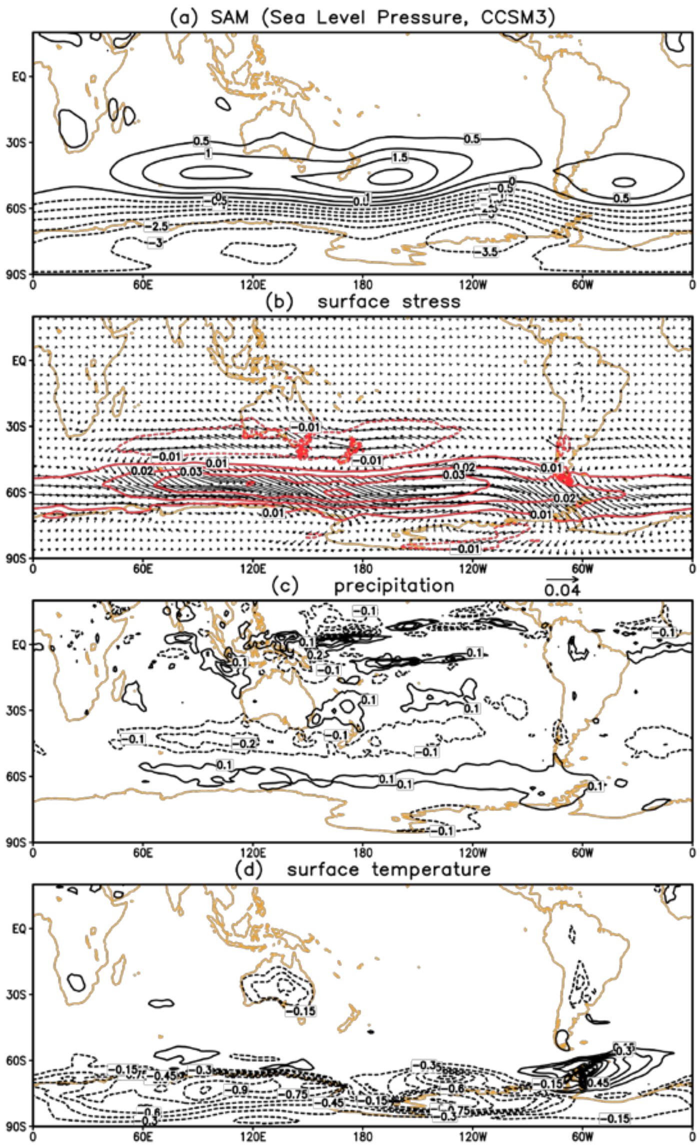

Figure 8. The same as Fig. 7, but for 200-year CCSM3/POP simulation with present-day forcing.

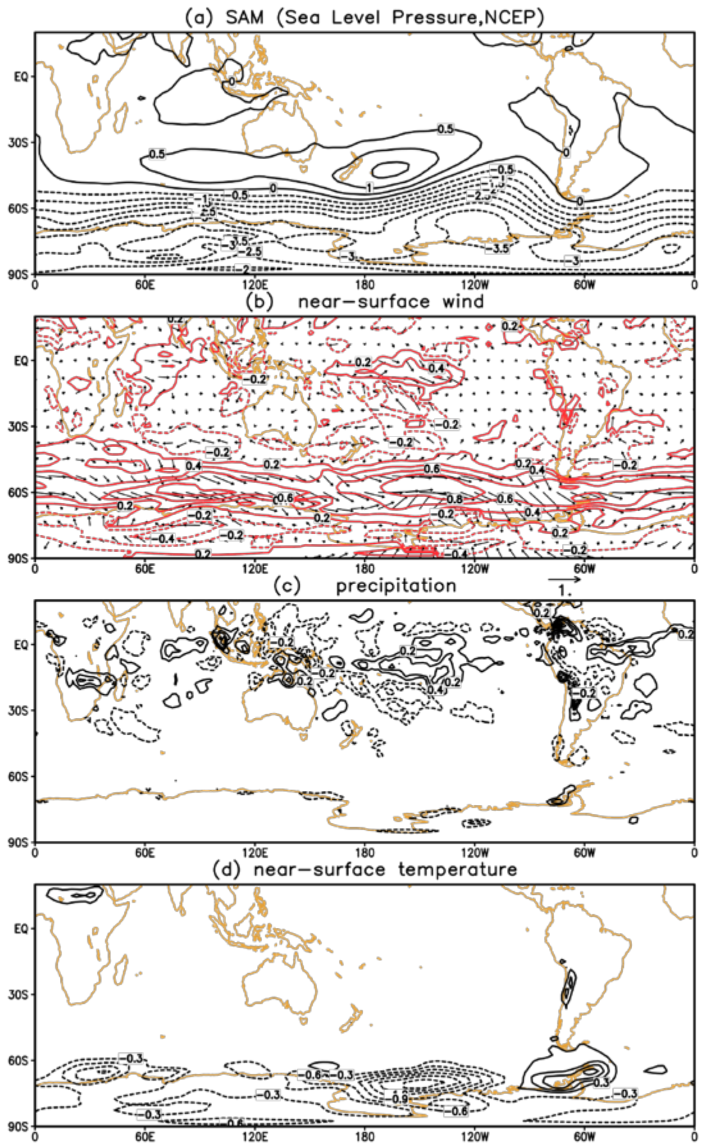

Figure 9. The same as Fig. 7, but with 60-year (1951-2010) NCEP/NCAR reanalysis data. The surface wind stress in panel (b) and surface temperature in (d) are replaced by wind and air-temperature at the lowest model level (σ=0.995).

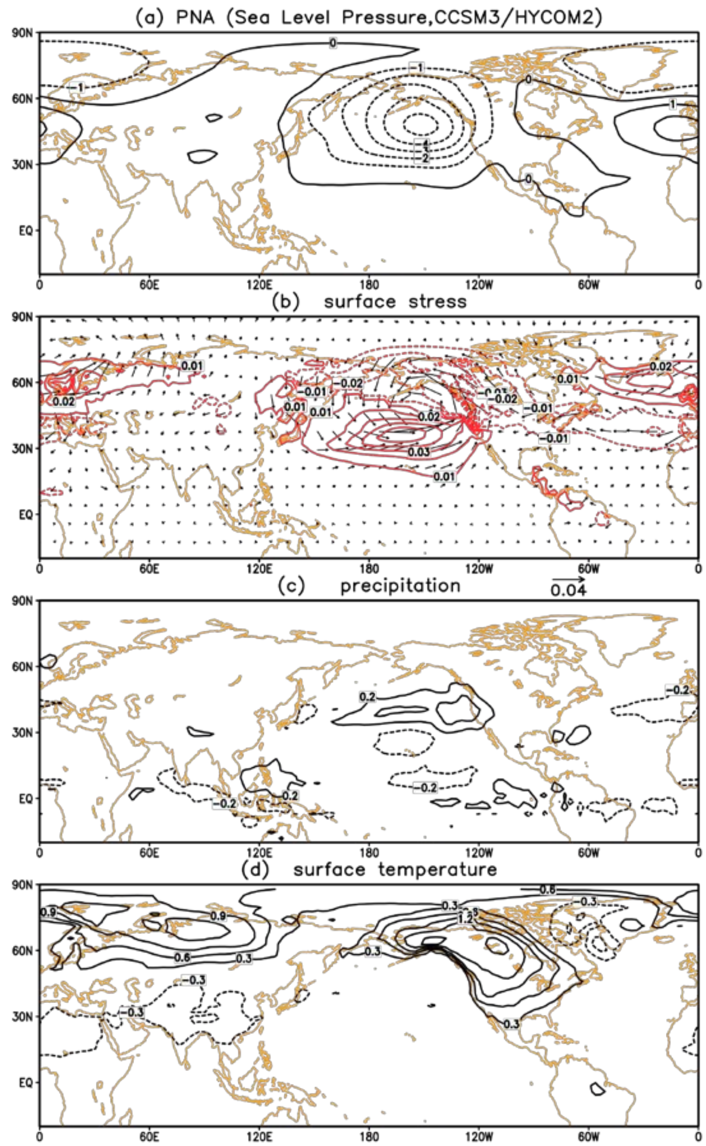

Figure 10. The PNA pattern - the second EOF of the October-to-March-averaged sea level pressure (SLP) over 20°N-90°N for 200-year coupled CCSM3/HYCOM simulations with present-day forcing (a). The linear regressions of surface wind stress (b), precipitation (c), and surface temperature (d) upon the PNA. The regressions are normalized by the standard deviation of the PNA mode.

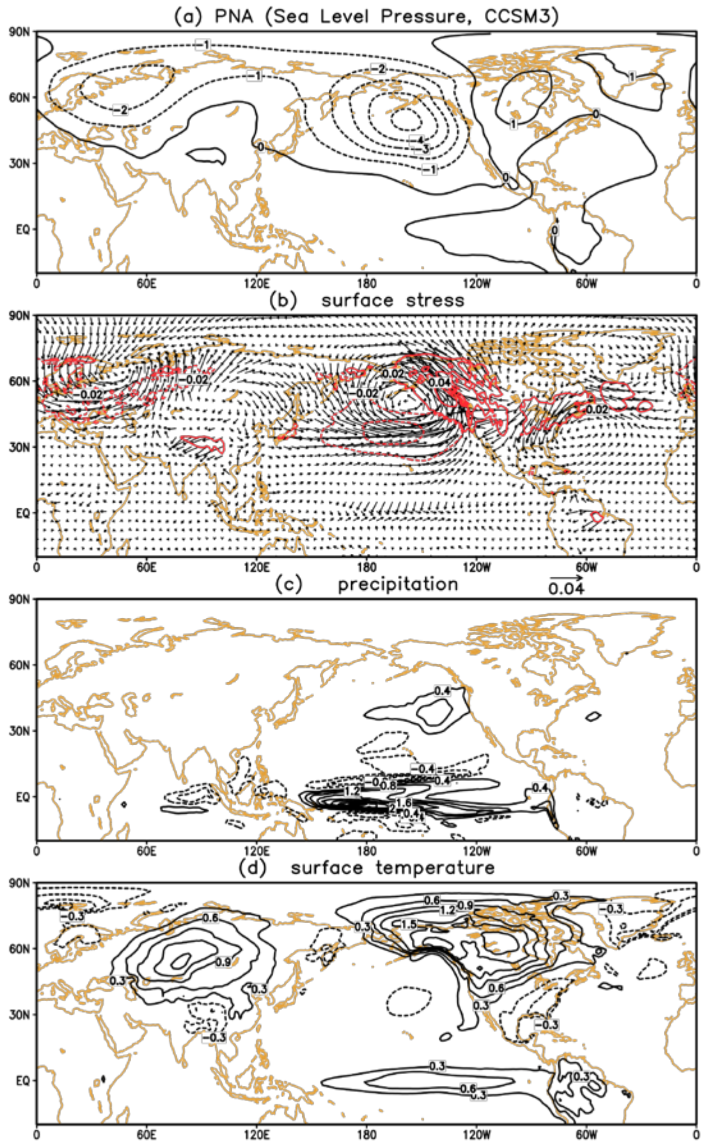

Figure 11. The same as Fig. 10, but for 200-year CCSM3/POP simulation with present-day forcing.

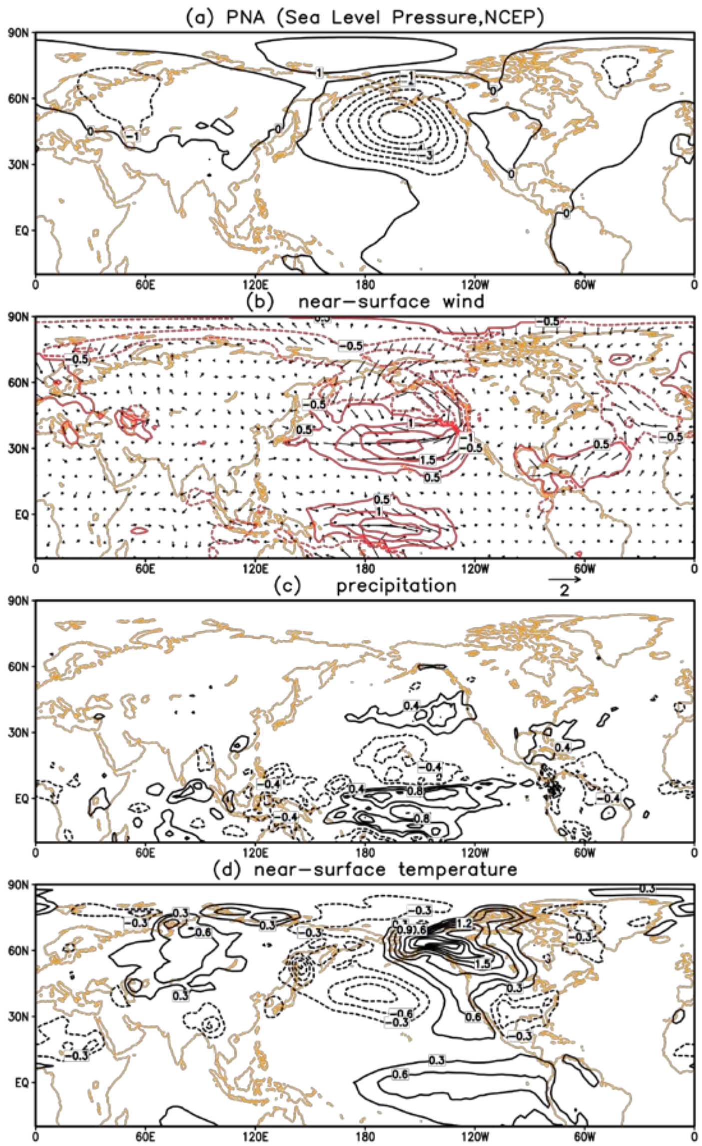

Figure 12. The same as Fig. 10, but with 60-year (1951-2010) NCEP/NCAR reanalysis data. The surface wind stress in panel (b) and surface temperature in (d) are replaced by wind and air-temperature at the lowest model level (σ=0.995).

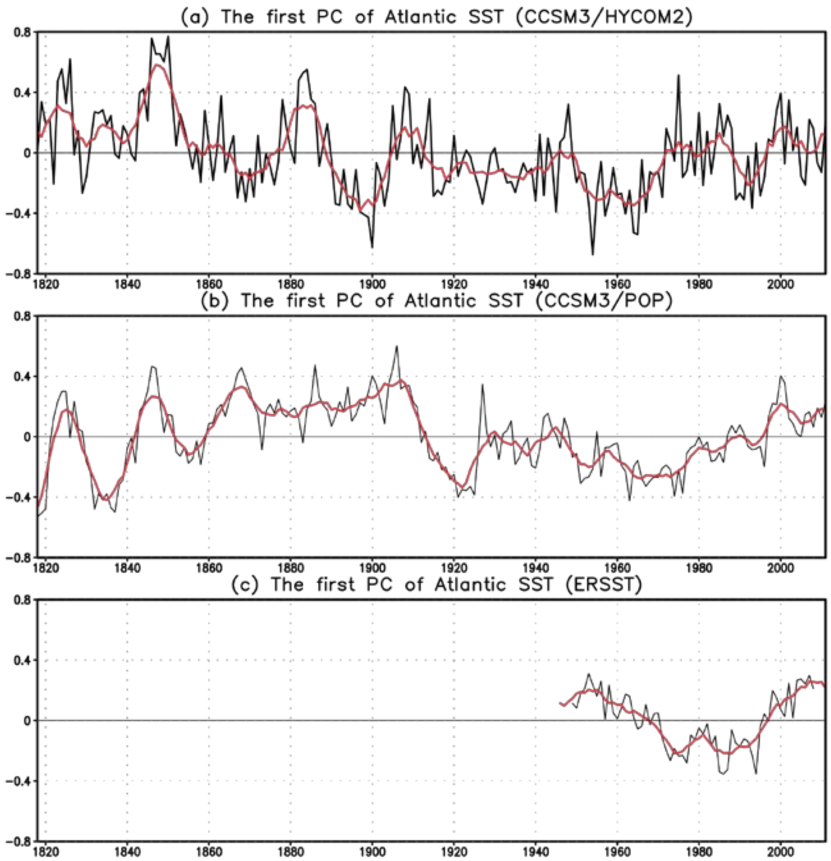

Figure 13. The time series of the AMO in CCSM3/HYCOM (a), CCSM3/POP simulations, and in observation (version 3 of ERSST data, Smith et al. 2008)

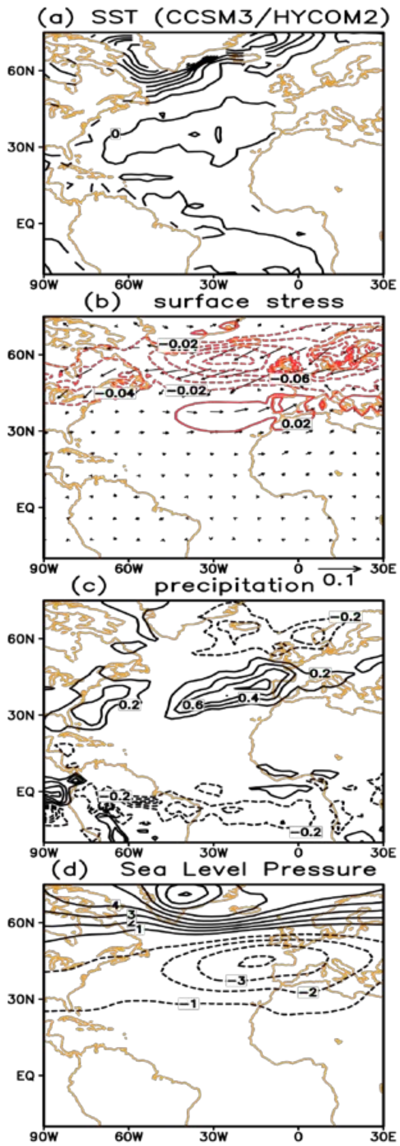

Figure 14. The AMO - the first EOF of the October-to-March-averaged SST over the North Atlantic (0-90°N) for 200-year coupled CCSM3/HYCOM simulations with present-day forcing (a). The linear regressions of surface wind stress (b), precipitation (c), and SLP (d) on the AMO. The regressions are normalized by the standard deviation of the AMO mode.

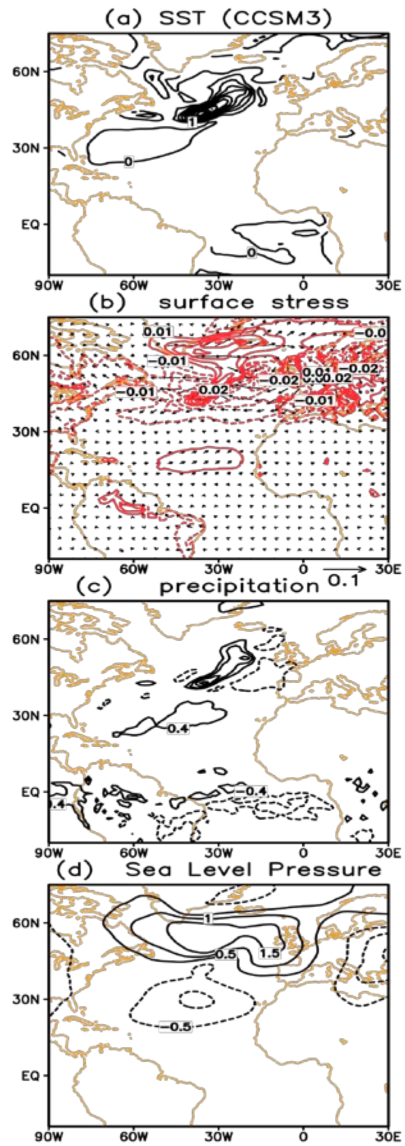

Figure 15. The same as Fig. 14, but for 200-year CCSM3/POP simulation with present-day forcing.

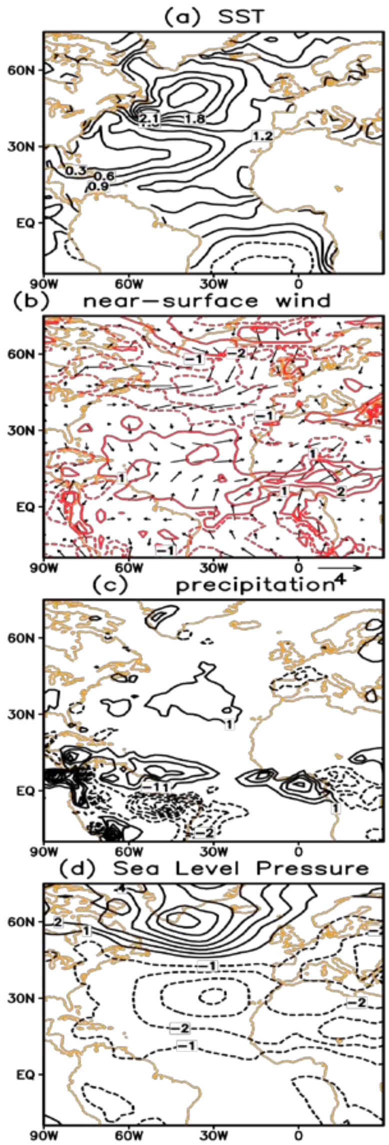

Figure 16. The same as Fig. 14, but with 60-year (1949-2008) ERSST data (a) and NCEP/NCAR reanalysis data (b-d). The surface wind stress in panel (b) is replaced by wind at the lowest model level (σ=0.995).

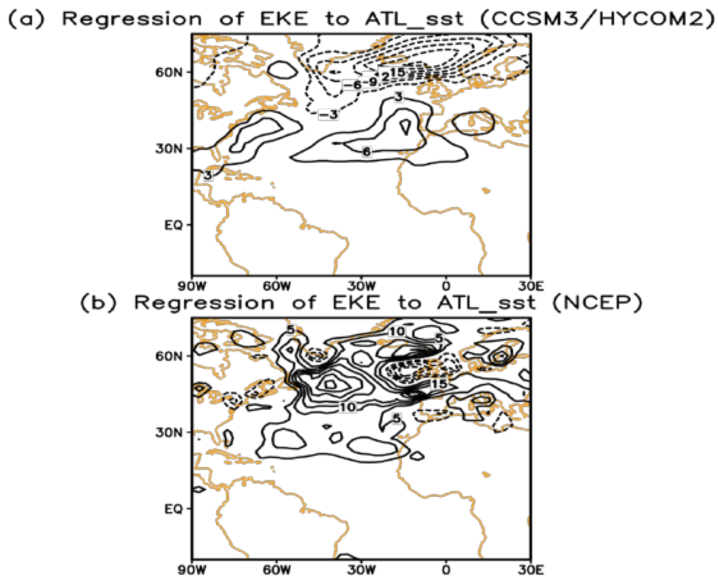

Figure 17. The linear regressions of EKE at lowest level upon the AMO in CCSM3/HYCOM simulation (a) and NCEP/NCAR reanalysis data (b), normalized by the standard deviation of the AMO mode. The data for CCSM3/POP simulation are not available.

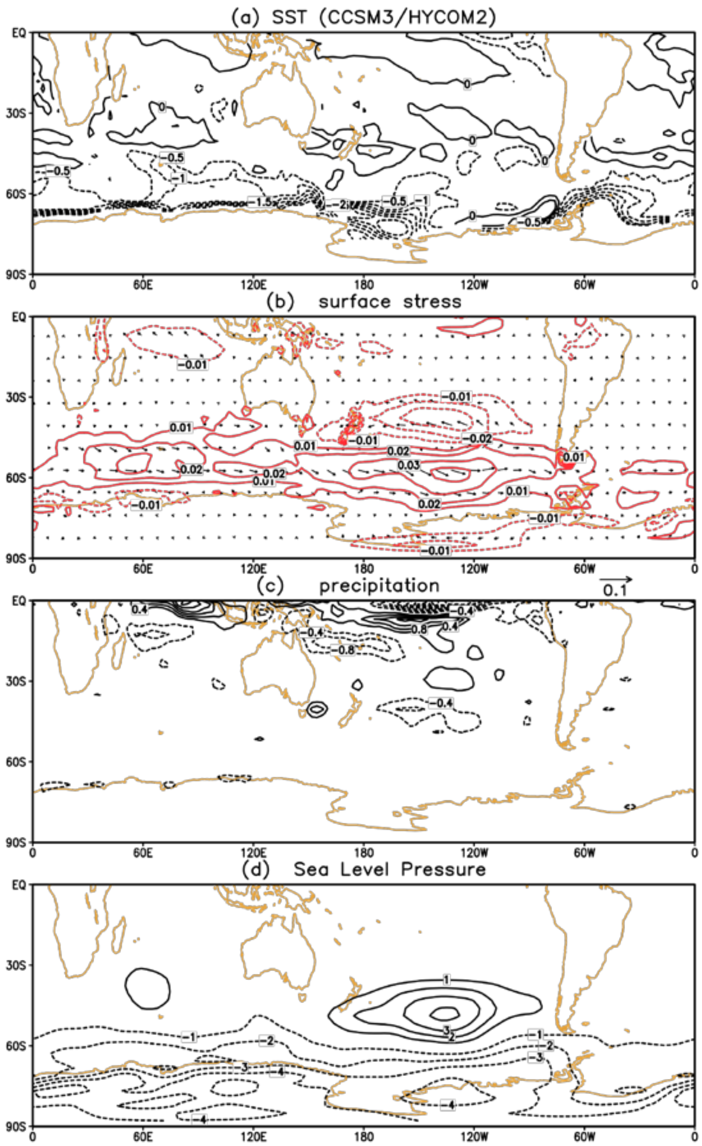

Figure 18. The first EOF of the April-to-September-averaged SST over the Southern Ocean (40°S-90°S) for 200-year coupled CCSM3/HYCOM simulations with present-day forcing (a). The linear regressions of surface wind stress (b), precipitation (c), and SLP (d) upon the SST mode. The regressions are normalized by the standard deviation of the SST mode.

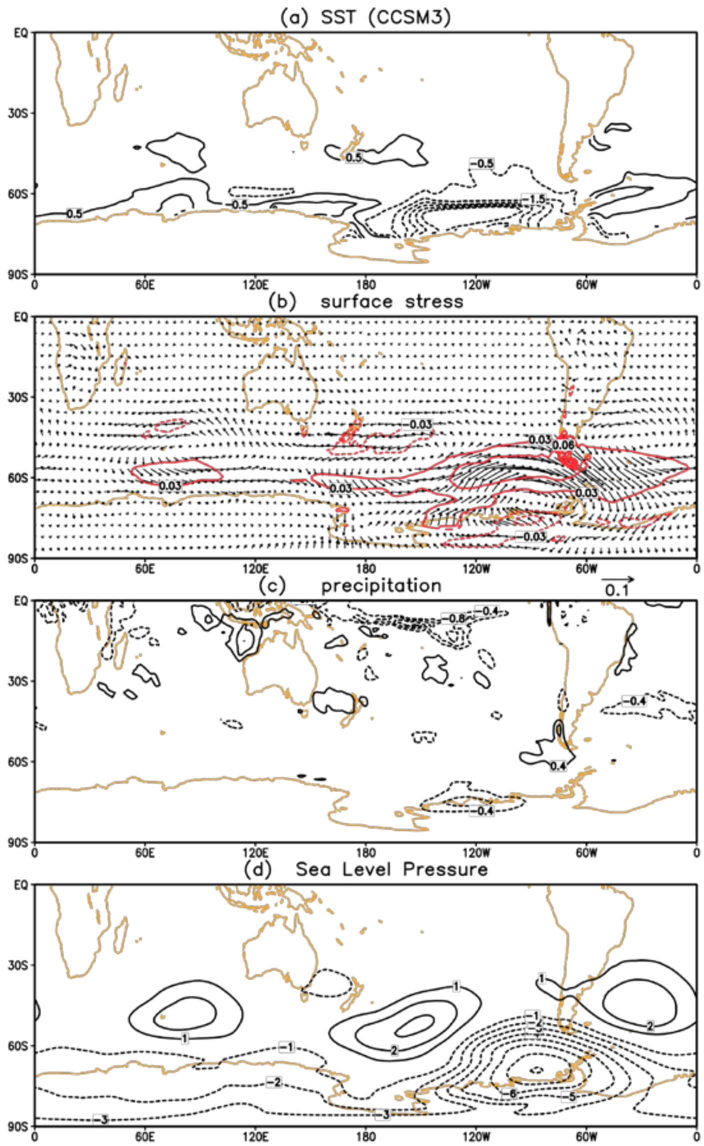

Figure 19. The same as Fig. 18, but for 200-year CCSM3/POP simulation with present-day forcing.

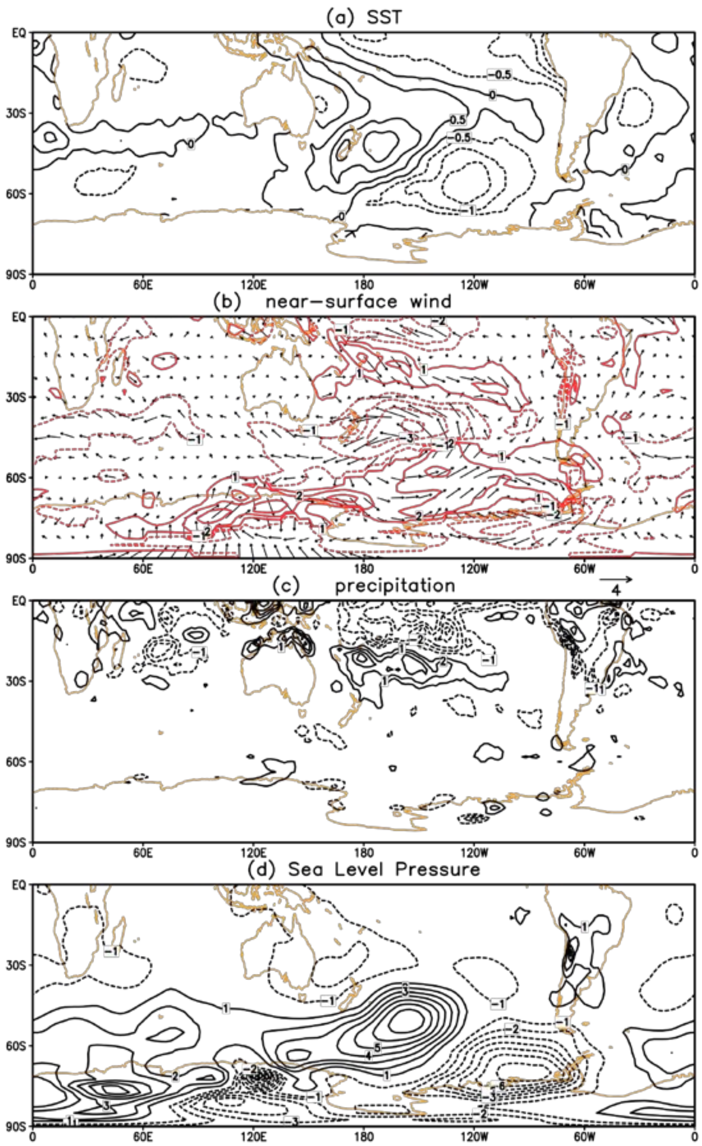

Figure 20. The same as Fig. 18, but with 60-year (1949-2008) ERSST data (a) and NCEP/NCAR reanalysis data (b-d). The surface wind stress in panel (b) is replaced by wind at the lowest model level (σ=0.995).